



A spatiotemporal teleconnection study between Peruvian precipitation and oceanic oscillations



Babak Mohammadi^a, Babak Vaheddoost^b, Ali Danandeh Mehr^{c,*}

^a State Key Laboratory of Simulation, Regulation of Water Cycle in River Basin, China Institute of Water Resources and Hydropower Research, Beijing, 100038, China

^b Department of Civil Engineering, Bursa Technical University, Bursa, Turkey

^c Department of Civil Engineering, Antalya Bilim University, Antalya, Turkey

ARTICLE INFO

Keywords:

Oceanic oscillations
Peru
Precipitation
Standardized precipitation index

ABSTRACT

Large-scale oceanic oscillations and their teleconnections with meteorological events are of great importance in macro-scale climatic studies. In this regard, this study investigates the spatiotemporal teleconnections between four oceanic oscillations, namely North Atlantic Oscillation (NAO), El Niño/Southern Oscillation (ENSO), Atlantic Multi-Decadal Oscillation (AMO), and Pacific Decadal Oscillation (PDO), against Peruvian precipitation patterns during the past 25 years (i.e., 1990–2015). For this purpose, variation in the precipitation pattern at monthly and annual scales as well as the Standardized Precipitation Index (SPI) time series at 1-, 3-, 12-, and 48-month time scales were evaluated at 10 meteorology stations across Peru. Pearson's correlation coefficient and mutual information between the oceanic oscillations and precipitation-born signals were calculated and spatially interpolated using the Kriging method. The results indicated the presence of three major climatic regions in the country. The NAO has the largest correlation with the monthly precipitation. However, the ENSO was found as the main climate driver of extremely wet and extremely dry conditions in the country. The results also demonstrated that the PDO has a higher impact on the annual precipitation pattern, particularly in the southern and eastern parts of the country.

1. Introduction

Precipitation, as the cornerstone of the hydrological cycle, is the main trigger of extreme weather/climate events such as droughts and floods. However, it is difficult to predict with long-term lead time (Danandeh Mehr et al., 2019). Recent studies have demonstrated that the large-scale climatic indicies and oceanic oscillations can be used as potential predictors of extreme weather events (Tong et al., 2006; Danandeh Mehr et al., 2017). For instance, Danandeh Mehr et al. (2014) showed that NINO 3.4 index has a robust effect in medium-to long-term drought events at the Texas State, USA. Huang et al. (2015) investigated the relationship between hydrological drought, climate indicators, and human activity in the Columbia River basin, USA. The results showed that the application of the maximum and minimum annual precipitations is inappropriate for checking the characteristics of frequency and magnitude of floods or droughts. Setiawan et al. (2017) studied the relationship between the ENSO and drought events in the Indonesian region and concluded that even severe seasonal droughts

could be predicted considering this index. Vaheddoost (2017) used several large scale oscillations including North Atlantic Oscillation (NAO), El Niño/Southern Oscillation (ENSO), Atlantic Multidecadal Oscillation (AMO), Arctic Oscillation (AO), Indian Ocean Dipole (IOD), Southern Annular Mode (SAM) and Pacific Decadal Oscillation (PDO) in the classification of annual precipitation over Lake Urmia Basin, Iran. Zeleke et al. (2017) used the Standardized Precipitation Index (SPI), the Palmer Drought Index (PDSI), and satellite data to investigate the drought in Ethiopia. The results showed that the observed dry and wet periods in the north of the country depend on the oscillations of the ENSO in spring and summer seasons. Yihdego et al. (2019) investigated the drought indices including SPI to conclude that the droughts should be evaluated based on the spatial and temporal expectations of a region rather than a global realization of this phenomena. Vazifehkhan and Kahya (2019) addressed the teleconnection between the hydrological and agricultural droughts at Konya Province of Turkey and several large-scale oscillations. Also, the recent study conducted by Danandeh Mehr and Vaheddoost (2019) investigated the applicability of SPI and

* Corresponding author.

E-mail addresses: babakmohammadi@aol.com (B. Mohammadi), babak.vaheddoost@btu.edu.tr (B. Vaheddoost), ali.danandeh@antalya.edu.tr (A. Danandeh Mehr).

Standardized Precipitation Evapotranspiration Index (SPEI) in Turkey at regional scale. The outcomes of the studies were projected as spatio-temporal thresholds in classification of the droughts severity as well as the associated historical trends. More recently, [Himayoun and Roshni \(2019\)](#) showed that the 3-month characteristics of SPEI are considerably influenced by the ENSO events throughout the Jhelum basin, India.

The Peruvian precipitation pattern, its drivers, and the teleconnection with oceanic oscillations have been investigated in many studies. For instance, a pioneer study conducted by [Thompson et al. \(1985\)](#) assessed the 1500-year climate of the country, based on the tropical Quelccaya ice cap samples taken from Mount Andes. [Tapley and Waylen \(1990\)](#) studied the annual rainfall at 18 meteorology stations distributed across northern Peru and the southern Altiplano. The authors concluded that the annual precipitations are under the influence of ENSO oscillation. [Shimada et al. \(1991\)](#), studied the role of climatic disturbances in northern Peru using annual precipitation record estimated from the ice cores from the Quelccaya glacier in southern Peru. It was concluded that the severest droughts of the past 1500 years were taken place between 562 and 594 AD. [Bendix et al. \(2000\)](#) used satellite data to investigate the spatial distribution of heavy precipitations in Ecuador and northern Peru during the 1991–1992 El Niño event. The results indicated the effectiveness of air fronts coming from the Pacific Ocean toward Mount Andes. It was also concluded that the ENSO has a great effect on the precipitation extremes in northern Peru. [Baker et al. \(2001\)](#) evaluated the 25000 historical precipitations in South America using sediment core samples of Lake Titicaca, Peru. [Lagos et al. \(2008\)](#) evaluated the monthly precipitation pattern at 44 meteorology stations across Peru. For this aim, the effect of mean sea surface temperature anomaly is addressed in the formation of El Niño and the regional classes approving the feasibility of the selected claim. [Condom et al. \(2011\)](#) and [Ochoa et al. \(2014\)](#) studied the spatial and temporal behavior of rainfall in Mount Andes. These regions were evaluated in comparison with the tropical rainfall measuring mission and correction models were suggested for this aim. [Perry et al. \(2014\)](#) studied precipitation, moisture, temperature, and wind speed in six stations across Peru between 2004 and 2010. Twice daily and hourly precipitation intensity from Cusco International Airport were used. It was concluded that the ENSO is not necessarily effective in the central Andes, while La Niña between 2007 and 2008 and El Niño between 2009 and 2010 caused in below normal and extreme precipitations respectively. [Zubieta et al. \(2015, 2017; 2019\)](#) studied the spatiotemporal variability of precipitation in different regions of Peru. [Viale and Nunez \(2018\)](#) studied the winter precipitations over Mount Andes at the western Peru concluding that the precipitation patterns of the region are connected with the presence of Mount Andes and water vapors coming from the Pacific Ocean. [Christidis et al. \(2019\)](#) investigated the March 2017 extreme precipitation event in Peru. It was concluded that the El Niño conditions in the coastal area together with the anthropogenic climate, exacerbate the extreme rainfall events in Peru. [Derin et al. \(2019\)](#) investigated the effect of Green House gases and climate change on precipitation extremes in several countries including Peru. It was concluded that the effect of climate change on precipitation extremes is various over different terrains. [Gonzalez et al. \(2019\)](#) investigated several mining regions and their vulnerability against climate change and extreme rainfall events in Peru. It was concluded that a decreasing trend can be associated with the rainfall extremes intensity and frequency, particularly in southern Peru. [Manzanas and Gutiérrez \(2019\)](#) used process-conditioned bias correction for seasonal precipitation forecasting, an empirical quantile-based mapping based on the Southern Oscillation Index (SOI) state was used. It was concluded that the large scale processes are relevant to the local climate and seasonal forecasting of precipitation. [Rodríguez-Morata et al. \(2019\)](#) evaluated extreme rainfall events during the austral summer of 2016–2017. The event was addressed with El Niño events of the last 40 years between 1982–1983 and 1997–1998. It was concluded that the changes in sea surface temperature at the eastern Pacific together with the El Niño events in 1982–1983, 1997–1998, and

2015–2016 were the main drivers of those extreme events. A recent study by [Vaheddoost \(2020\)](#) showed that the Andes has a major role in the climate of Peru. The ENSO and the PDO have a great effect on the extreme precipitations. It was also concluded that precipitation increases from west to the east of the country, while there is a decreasing pattern in precipitation at the Amazon rain forests.

The aim of this study is, for the first time, to investigate the spatio-temporal teleconnections between the recent Peruvian precipitations (1990–2015) and oceanic oscillations that occur around the country. The study is accomplished in different time horizons of monthly and annual scales in terms of teleconnection on precipitation pattern as well as the 1-, 3-, 12-, and 48-month time scales to assess the potential teleconnections between the oceanic cycles and SPI as the signal of prolonged dry and wet spells across Peru. It is also aimed that the obtained results would be useful for extreme weather management of the country.

2. Study area and data

Peru is located between 0° and 18° southern latitude and 69°–81° western longitude ([Fig. 1](#)). It has a coastline along with the Pacific Ocean and borders with Ecuador, Colombia, Brazil, Chile, and Bolivia. The main geomorphological features of the country include the *Costa* (western coasts near the Pacific), *Sierra* (the highlands of the Mount Andes and Altiplano), and *Selva* (Amazon rainforests) shared with Brazil and Colombia (see [Fig. 1b](#)). Based on the Köppen-Geiger climate classification, there are four major and 15 minor climate classes across the country. The major classes are the tropical, arid, temperate, and polar, and the minor ones comprise the humid (Af), equatorial monsoonal (Am), equatorial desert (Aw), arid desert-hot (BWh), arid desert-cold (BWk), arid steppe-hot (BSh), arid steppe-cold (BSk), temperate dry-warm summer (Csb), temperate dry-cold summer (Csc), temperate dry-winter and warm-summer (Cwb), temperate dry-winter and cool-summer (Cwc), temperate humid and warm-summer (Cfb), temperate humid and cool-summer (Cfc), polar tundra (ET), and polar forest (EF) sub-classes ([Kottek et al., 2006; Beck et al., 2018](#)). There are also several micro-climate classes which could be observed at catchment scale across the country. In this respect, the Peruvian climate is influenced by the surrounding ocean and landforms and thereby, the spatiotemporal teleconnection analysis between large-scale oscillations and the precipitation patterns would be informative for water resources management in the country.

2.1. Precipitation and Standardized Precipitation Index (SPI)

The daily precipitation data from 16 meteorology stations were gathered from the Republic of Peru National Service of Meteorology and Hydrology (SENAMHI). As shown in [Fig. 2](#), ten of these stations, namely El Salto in Tumbes (TMB), Granja Kcayra in Cusco (CUS), Recuay in Ancash (ANC), Imata in Arequipa (AQP), Matucana in Lima (LIM), San Ramon in Loreto (LSR), Sama Grande in Tacna (TAC), El Maronal in Ucayali (UCA), Lamas in San Martin (SAM), and Cayalí in Lambayeque (LAM), had long-term high-quality measurements during the period of January 1, 1990, to October 31, 2015. Therefore, they have been selected to be evaluated in this study. Consistency of the measurements at these stations has already been proved by [Vaheddoost \(2020\)](#) using double mass curve analysis.

Main statistical characteristics of the observed precipitation time series are tabulated in [Table 1](#). The table indicates that the highest mean and standard deviation belongs to the LSR, which is located at the Amazon region. This is due to the frequent rainfall events which take place in the tropical rain forest. The LAM station has the minimum monthly precipitation and also shows the highest skewness and kurtosis among the probability distributions associated with the data at the selected stations. This particularly means that tropical rainforests have the highest precipitations whilst the western coasts experiences large variation in precipitation since they are under influence of air fronts

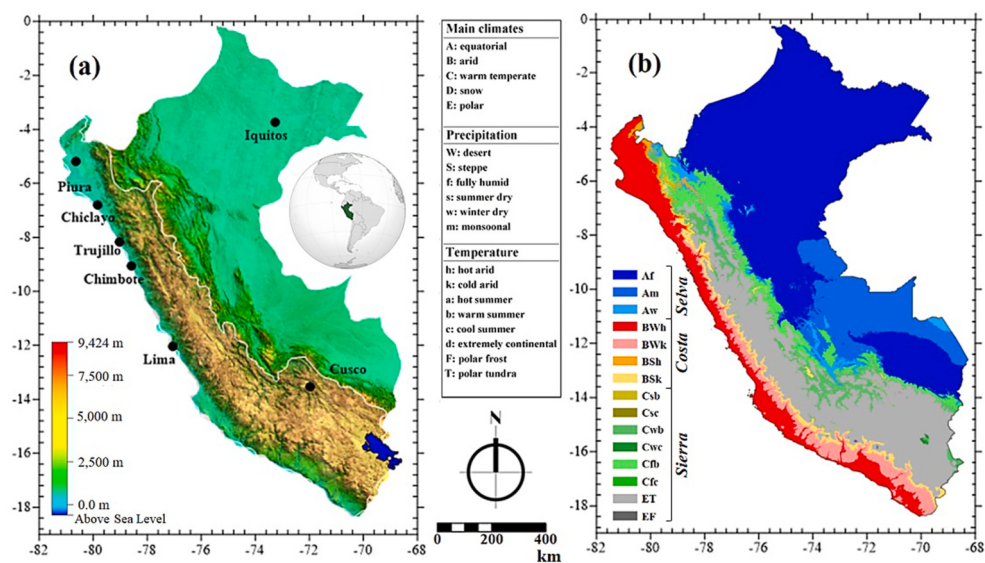


Fig. 1. Peru map including (a) location of the cities and features, and (b) major climate-regions based on Köppen-Geiger climate classification.

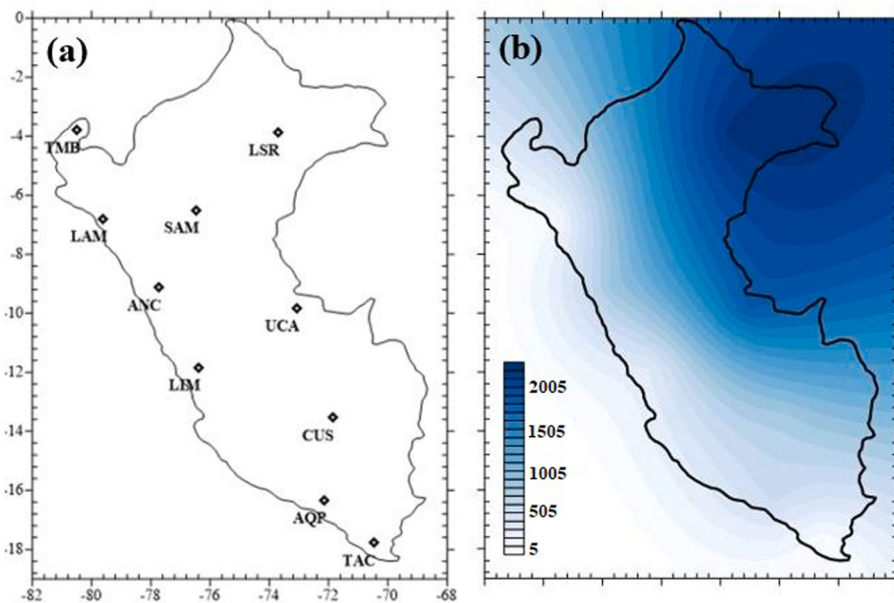


Fig. 2. (a) Location of the selected stations across Peru and the (b) mean annual precipitation map.

Table 1

Main statistical characteristics of total monthly precipitations at the selected stations for the period 1990–2015.

Station	Acronym	Mean (mm)	Std. Dev. (mm)	Skewness (-)	Kurtosis (-)
El Salto	TMB	1.40	8.92	5.36	39.95
Granja Kcayra	CUS	2.11	4.89	0.89	2.92
Recuay	ANC	2.26	4.48	0.96	3.46
Imata	AQP	1.44	3.99	1.40	4.09
Matucana	LIM	0.87	2.45	1.51	4.74
San Ramon	LSR	6.17	13.72	0.95	4.56
Sama Grande	TAC	0.07	0.43	5.79	42.72
El Maronal	UCA	5.02	13.12	0.89	3.63
Lamas	SAM	3.67	8.84	0.78	3.71
Cayalti	LAM	0.21	1.88	9.79	120.27

coming from the Pacific and the harsh conditions of the Andes.

2.2. The large-scale oceanic oscillations

The oceanic oscillations are periodic or semi-periodic phenomena with interannual and/or interannual periodicity and may form extreme weather condition (flood, drought, tornado, etc.) in different regions. Hence, they are thought to be effective climatic drivers for dry and wet periods that took place in Peru. For this aim, four well-known oceanic oscillations, namely the North Atlantic Oscillation (NAO), El Niño/Southern Oscillation (ENSO), Atlantic Multi-decadal Oscillation (AMO), and Pacific Decadal Oscillation (PDO) that respectively take place at northeast, west, east, and northwest of Peru were used in this study for teleconnection analysis. Fig. 3, shows the location of these oscillation and their corresponding monthly mean indices during the 1990–2015 period which were retrieved from the National Oceanic and Atmospheric Administration (NOAA) website (<https://www.esrl.noaa.gov/>).

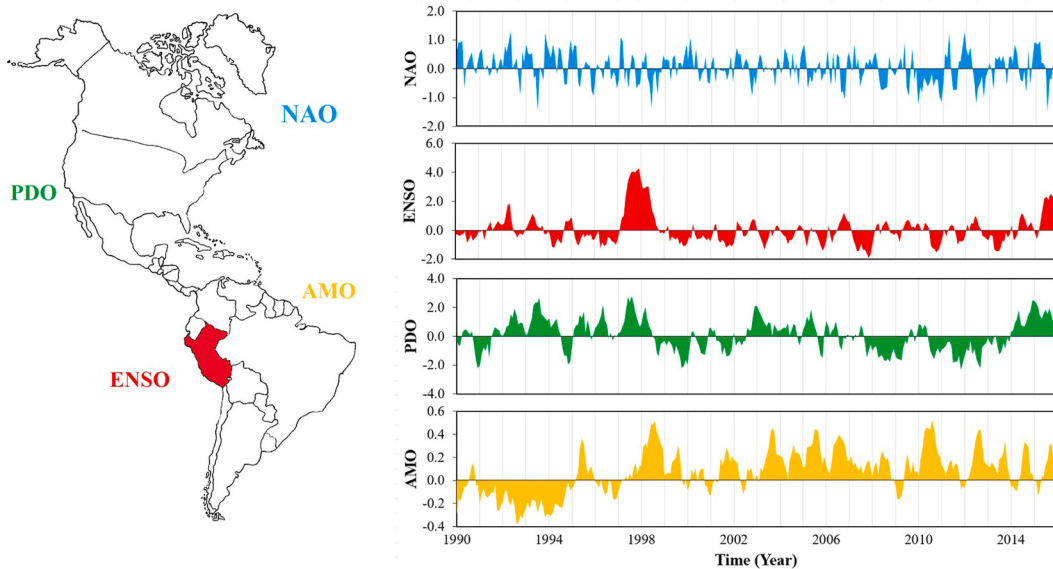


Fig. 3. The location and monthly mean time series of the selected large-scale oscillations.

The NAO index corresponds to the sea surface pressure and the difference between the Icelandic low and Azores high over the subtropical zone (Vaheddoost, 2017). The positive and negative phases of the NAO respectively indicate the below-normal and above-normal pressure anomalies in the North Atlantic Ocean. It is linked to the basin-wide changes over the intensity and location of the jet streams, storms, and large-scale changes in the zonal and the meridional heat and moisture transport. This phenomenon causes changes in the temperature and precipitation patterns between northern America and central Europe. The ENSO index corresponds to the El Niño-Southern Oscillation which is a recurring climate pattern involving changes in the sea surface temperature in the central and eastern tropical Pacific Ocean. Based on the warming and cooling of the ocean surface temperature, there are two opposite phases of the ENSO cycle called *El Niño* and *La Niña*, respectively. These are extreme phases of the ENSO cycle and the normal phase between these two phases is called ENSO-neutral. Each phase affects rainfall distribution in the tropics and other parts of the world in different ways. The AMO is a prominent pattern of climate variability that occurs in the North Atlantic Ocean with an approximate period of

60–80 years. The AMO index corresponds to a quasi-periodic cycle in the thermohaline circulation that changes the ocean surface temperature. When the AMO phase is positive, the water circulation in the ocean moves faster, and the westerly winds of the mid-latitude shift northward. On the other hand, during the negative phase of AMO, the thermohaline circulation decreases, and the westerly winds shifts toward the south. The PDO is a recurring pattern of ocean-atmosphere climate variability centered over the mid-latitude Pacific Ocean. The extreme PDO events, oscillate the climate of the Pacific Ocean and North America. Together with the ENSO, the extreme phases of PDO are under influence of sea surface temperature anomalies. The sea surface temperature anomaly is considered as cool in the north Pacific and warm along the Pacific Coasts. When the sea level pressure is low, PDO is in a positive phase; however, when the climate anomaly patterns are reverse, the PDO is in a negative phase.

3. Methodology

Fig. 4 illustrates the proposed methodology applied to explore the

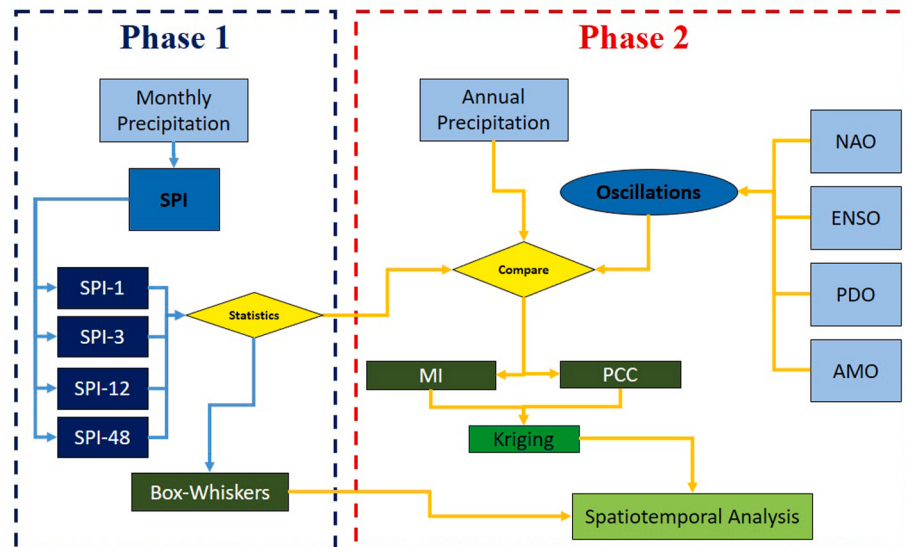


Fig. 4. The proposed methodology for the teleconnection study between precipitation and climate oscillations.

teleconnection between characteristics of the Peruvian precipitations and the large-scale oceanic oscillations. In the first phase, the SPI as the well-known signal of prolonged wet and dry spells (i.e., surplus and deficit condition in monthly precipitation) is calculated for describing the precipitation pattern across the country. The SPI is calculated in four time scales of 1- (hereafter SPI-1), 3- (hereafter SPI-3), 12- (hereafter SPI-12), and 48-months (hereafter SPI-48) in order to characterize the monthly, seasonal, annual, and long-term precipitation patterns, respectively. These are time horizons that also were suggested to evaluate the situation of precipitation, soil moisture, permanent water reservoirs, and climate of a region (Yihdego et al., 2019). The Box-Whiskers plot of the SPI indices were then depicted to explore the spatiotemporal variation of wet and dry spells with respect to the thresholds given in Table 2.

In the second phase, the teleconnection between different phases of NAO, ENSO, PDO, and AMO and monthly and annual precipitations as well as SPI at 1-, 3-, 12-, and 48-month moving averages (MA) are analyzed using Pearson's correlation coefficient (PCC) and mutual information (MI) theory. Finally, the obtained results were projected on the country map using Kriging method which provides insight about the spatial version of the potential teleconnections. In this regard, the provided results depict a deterministic and a stochastic overview on the relationship between the selected large-scale oscillations and the drought events at selected stations.

It is noteworthy that the PCC only depicts the linear relationship (i.e. deterministic approach), however the MI which measures the mutual dependency of the variables is a good measure of nonlinear correlation (i.e. stochastic approach). The MI is based on the joint probability of paired sample and is expressed as below.

$$MI[SPI(X), Index(Y)] = \sum_{x=1}^7 \sum_{y=1}^2 P(x,y) \log_2 \left(\frac{P(x,y)}{P(x)P(y)} \right) \quad (1)$$

where MI between SPI of the allocated time frame (i.e. MA) and the phase of the selected oscillation (i.e. NAO, ENSO, AMO, or PDO) were compared with each other. In this statement, x is an outcome related to the degree of the SPI classes; whilst, y is the outcome of the positive (+) or negative (-) phases of the selected oscillation at the allocated time frame.

4. Results and discussion

Fig. 5 depicts the SPI signals at each station for 1-, 3-, 12-, and 48-month time scales. As highlighted by WMO (2012), the SPI is the best meteorological drought index that indicates prolong deficit in precipitation if it receives negative value. **Fig. 5a** shows that an extreme wet condition occurred in late 1998 while, there is a sign of an emerging drought in late 2015. The SPI-3 however, showed no significant difference compared to the results of SPI-1 (**Fig. 5b**). On the other hand, several drought spells were emerged in SPI-12 and SPI-48 which were neither detectable in SPI-1 nor in SPI-3. This is a clear sign for significant annual variations. On a larger scale however, the sign of drought in late 2015 was emerged (**Fig. 5c** and d) which could not be compared with the historical events. This may be due to climate change or a macro-climate patterns that are emerging over the country. The monthly average SPI

(SPI-1) value is also given in **Table 3** which clarifies the situation of the interannual wet and dry spells in the selected stations. In TMB and ANC, the precipitation deficit occurs in July; whilst the stations CUS, LSR, SAM, and LAM experience deficit in August. In AQP and UCA, June is the driest season while the LIM station experience a continuous deficit extending from June to August. In TAC station however, no sign of deficit was observed. On the other hand, the SPI-1 values in all station except TAC shows that the positive values of SPI-1 occur between January to April while the remaining months of the year are mostly under the effect of negative SPI-1 or near normal values. In this respect, the SPI-1 values in TAC stations shows positive values near the Lake Titicaca all the time, that partially indicates to a continuous surplus in the region.

The frequency of the SPI patterns is also given in Box-Whiskers plot in **Fig. 6**. The SPI-1 patterns (**Fig. 6a**) shows that most of the stations experienced moderately to extremely wet spells. Particularly, in TMB, AQP, LIM, and TAC station the SPI-1 values are positively skewed which indicates to an ongoing surplus in the precipitations. However, in the remaining stations, a moderate negative skewness was observed. The SPI-3 value in **Fig. 6b** however, shows that at seasonal scale some deficit emerges and extreme drought events can be recognized. In larger time scale, the SPI-12 (**Fig. 6c**) and SPI-48 (**Fig. 6d**), deficit events exceeded the surplus events. In this respect, moderate or near normal surplus at the monthly scale transforms into extreme drought events at large-scale time frame. Particularly at 2015, the precipitation deficit was accelerated in all of the stations (**Fig. 6d**). The most extreme event, however, took place at UCA and SAM which are located at the eastern Andes (**Fig. 6d**). Thereby, it can be interpreted as the changing climate or effect of large-scale atmospheric oscillations in the Amazon.

As illustrated in **Fig. 4**, the effect of selected large-scale oscillations, i.e. NAO, NSO, AMO, and PDO, on the SPI-1 was investigated in the second phase. In **Fig. 7**, the correlation between monthly and annual precipitation with selected oscillations are given. Accordingly, the thresholds for the significance of correlation coefficients at monthly and annual scales are 0.11 and 0.38, respectively. Based on the analysis, it seems that the NAO oscillation (**Figs. 7a-1** and **7a-2**) has a maximum correlation coefficient of 0.40 with the monthly precipitation time series. In this respect, monthly precipitation has a significant linear relationship with the NAO index, while such bound could not be reproduced at an annual scale. The ENSO oscillation also has some serious effects in the northwest and southwest of the country (**Figs. 7b-1** and **7b-2**). With respect to the annual scale variation, there are signs of interconnection with precipitation in the eastern parts of the country. Therefore, the ENSO time series both at monthly and annual scale depicts similarities with precipitation at the selected stations. Similarly, the correlation coefficient between the PDO index and precipitation (**Figs. 7c-1** and **7c-2**) demonstrates that the PDO has a significant effect on the annual and monthly precipitations of the southern and eastern parts of the country. The AMO oscillation almost has no significant correlation on precipitation at a monthly scale whilst the mountainous ranges (**Figs. 7d-1**) and eastern parts of the country have moderate correlations with annual precipitations (**Figs. 7d-2**). Hence, the results obtained at the monthly scale do not confirm the obtained results for the annual scale. However, the effect of Mount Andes both at annual and monthly scale is depicted which is in total agreement with the results of Condom et al. (2011), Ochoa et al. (2014), and Viale and Nunez (2018). In this respect, three different regions emerged that is located on the western, central, and eastern Andes.

The spatiotemporal teleconnection between NAO, ENSO, PDO, and AMO indices with the SPI-1 index is presented in **Fig. 8**. The PCC and MI were used to realize the linear and mutual dependency between pair samples of SPI-1 and a desired large-scale oscillation. Thereby, MI values shows the joint probability of outcome in SPI and the selected oscillation. Although the PCC between the NAO and the SPI-1 was partially significant in most of the country (significant PCC: 0.11), it was found to be positive for the entire country. The highest PCC and MI were

Table 2
SPI threshold considered in this study (McKee et al., 1993).

Threshold	Drought Spell
SPI ≥ 2.0	extremely wet
2.0 > SPI ≥ 1.50	very wet
1.50 > SPI ≥ 1.00	moderately wet
1.00 > SPI ≥ -1.00	near normal
-1.00 > SPI ≥ -1.50	moderately dry
-1.50 > SPI ≥ -2.00	severely dry
SPI ≤ -2.0	extremely dry

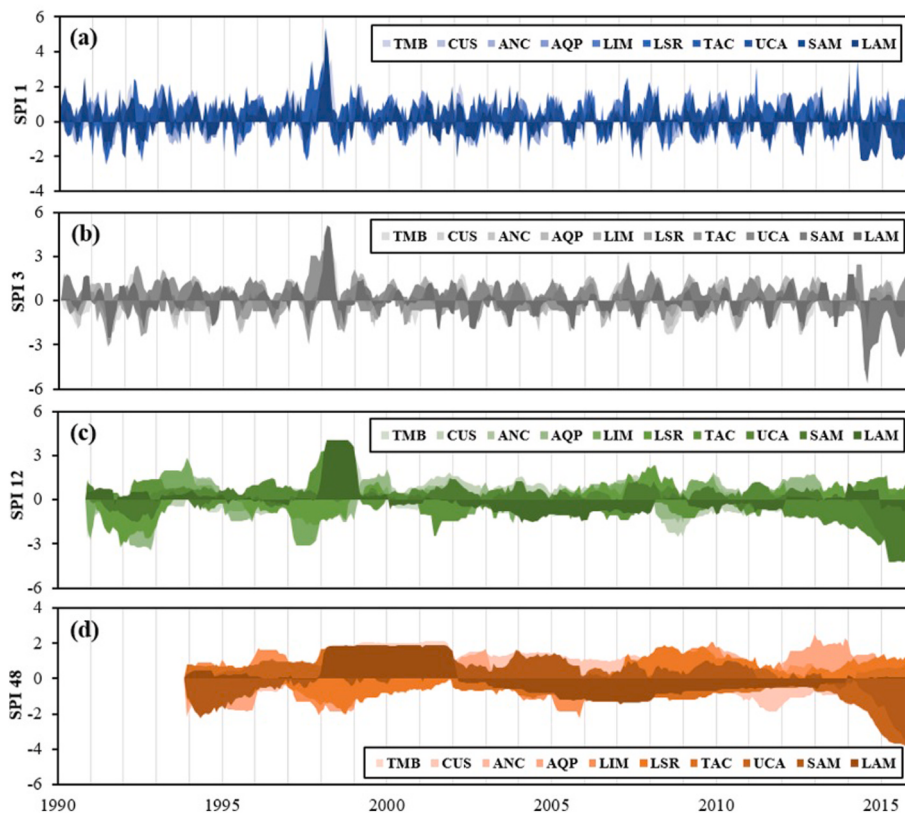


Fig. 5. Time series of SPI at (a) 1-month, (b) 3-month, (c) 12-month, and (d) 48-month time scale.

Table 3

The average monthly SPI (SPI-1) patterns.

Station Month	TMB	CUS	ANC	AQP	LIM	LSR	TAC	UCA	SAM	LAM
Jan	0.59	1.09	0.75	1.31	0.96	0.13	0.38	0.92	0.07	0.37
Feb	1.13	1.04	0.81	1.20	1.16	0.46	0.22	0.33	0.36	0.77
Mar	1.11	0.75	1.20	0.99	1.30	1.05	0.24	0.12	0.71	1.00
Apr	0.61	0.20	0.57	0.26	0.41	0.51	0.45	-0.43	0.55	0.56
May	-0.01	-0.51	-0.31	-0.59	-0.33	-0.15	0.34	-0.93	0.16	-0.26
Jun	-0.32	-0.74	-0.97	-0.73	-0.37	-0.54	0.45	-0.86	-0.41	-0.54
Jul	-0.48	-0.64	-1.18	-0.69	-0.37	-0.89	0.50	-0.37	-0.30	-0.75
Aug	-0.37	-0.75	-0.98	-0.57	-0.37	-1.05	0.74	-0.20	-0.75	-0.83
Sep	-0.42	-0.38	-0.36	-0.47	-0.32	-0.45	0.73	0.36	-0.08	-0.24
Oct	-0.34	0.00	0.33	-0.19	-0.01	0.09	0.45	0.31	0.20	0.06
Nov	-0.36	0.17	0.35	0.03	0.12	0.51	0.37	0.38	0.12	-0.01

observed in the southwest of the country near the LAM and AQP stations. The ENSO oscillation also showed a positive and significant correlation in the southern parts of the country near the location in which the oscillation occurs. Based on the MI results, the highest teleconnection is observed at SAM station (see Figs. 8c–2). Considering the results of ENSO, they can be compared with the results of Tapley and Waylen (1990), Bendix et al. (2000), Lagos et al. (2008), Perry et al. (2014), Christidis et al. (2019), and Rodríguez-Morata et al. (2019) who defined the different climatic areas under the effect of ENSO in the Peru. Similarly, PDO oscillation had no significant correlation with any stations except SAM which is located at the central Amazon. Therefore, the tropical precipitations in the Amazon were also under the influence of sea surface temperature in the Pacific Ocean. The impact of AMO, similarly showed a low degree of significance. However, the coasts at southwest and near the Pacific Ocean, seem to have an inverse relation with AMO. Based on the MI analysis, selected oscillations have a great influence on LIM and UCA stations (see Figs. 8d–2). Hence, the

information depicted by the deterministic PCC shows that the nature of relationship between SPI-1 and oscillations are not significant, while the stochastic MI shows that regional events may be under the influence of selected large-scale oscillations.

Similarly, the deterministic and stochastic relationships between the SPI and selected oscillations are investigated at 3- (Fig. 9), 12- (Fig. 10), and 48-month (Fig. 11) by considering the PCC and MI of the allocated MA time series. The threshold PCC for the 3-, 12-, and 48-MA analysis are respectively 0.11, 0.11, and 0.12. To this end, in Figs. 9a–1, 10a–1, and 11a–1 the PCC between SPI-3 and 3-month MA of NAO is depicted. Although the results of SPI-1 and SPI-3 in Figs. 8a–1 and Figs. 9a–1 are more or less similar, by consideration of SPI-12 and SPI-48 several hot spots emerged at the north and the south of the country. The same results for PCC analysis can be observed between Figs. 9b–1, 10b–1 and 11b–1 for ENSO; Figs. 9c–1, 10c–1 and 11c–1 for PDO; and Figs. 9d–1, 10d–1 and 11d–1 for AMO. In general, by widening the time frame, the PCC and MI increase. This clearly indicates the significant relationship

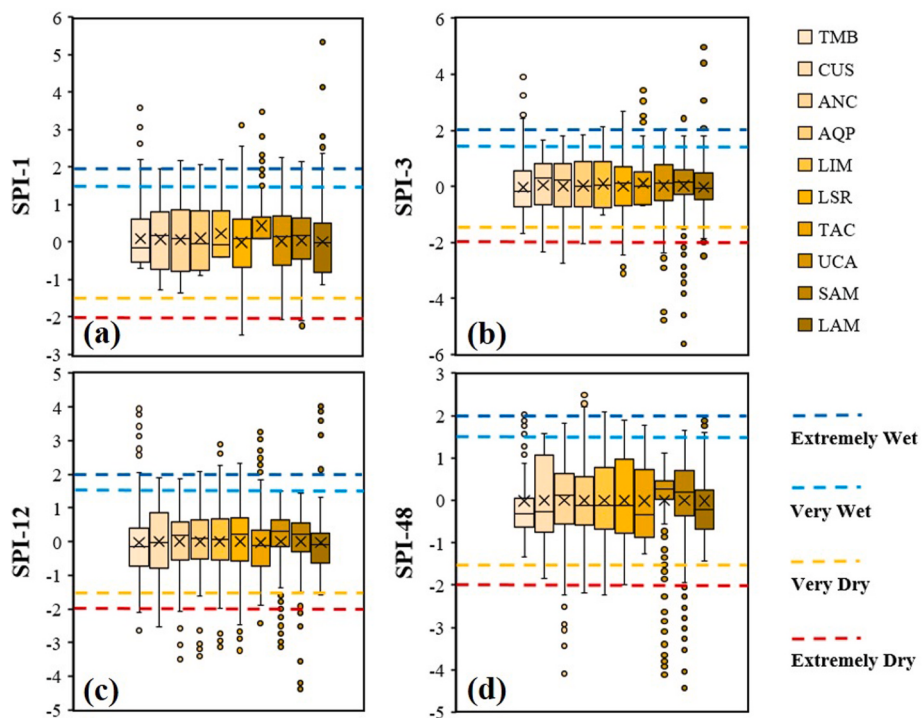


Fig. 6. The Box-Whiskers plot of the SPI at (a) 1-month, (b) 3-month, (c) 12-month, and (d) 48-month scale.

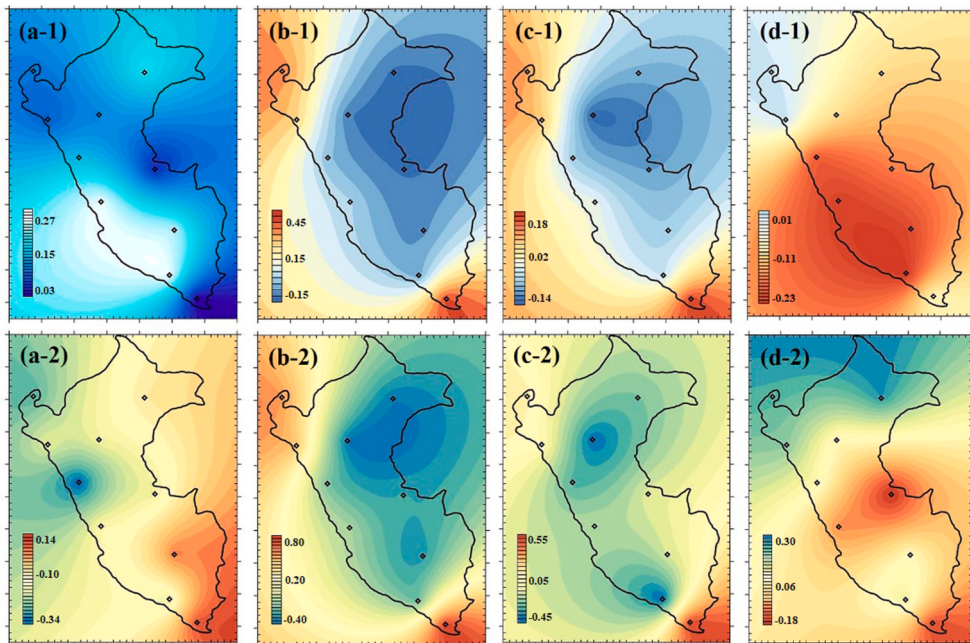


Fig. 7. Spatial effects of large-scale oscillation considering the PCC of precipitation with (a) NAO, (b) ENSO, (c) PDO, and (d) AMO at (1) monthly, and (2) annual scales.

between large-scale oscillations and precipitation at the allocated time frame. Accordingly, most of the large-scale oscillations at MA-48 showed significant PCC and MI values indicating the strong bond between the allocated variables. Therefore, by considering the relationship between SPI-48 and MA-48 in the oscillations, the ENSO in the north of the country (Fig. 11b) and PDO at the west of the country (Fig. 11d) triggers the drought events.

Fig. 12 is an illustration of the station based, temporal variations in the teleconnection between the oceanic oscillations and SPI-1, which is

the starting point for the analysis. It depicts the positive and the negative phases of the oscillations together with the deficit and surplus in the precipitation considering the SPI-1, drought index. Thereby, it is concluded that the extremely wet and extremely dry events occur when at least two of the oscillations have similar phases. Particularly, in the most extreme cases, all of the oscillations were positive and resulted in the most extreme wet spells at March 1992 in TMB; September 1997 in TAC; April 1998 in TMB; February 1999 in CUS, LIM in TMB; March 2002 in TMB; and December 2007 in UCA stations. These results confirm

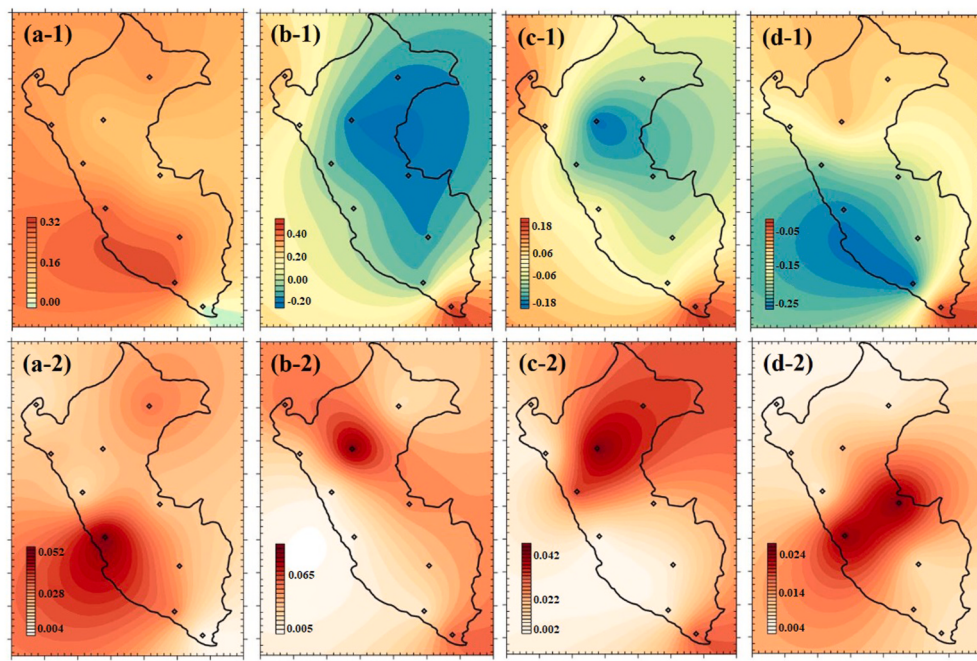


Fig. 8. The relationship between SPI-1 and NAO (a), ENSO (b), PDO (c), and AMO (d) by considering the (1) PCC and (2) MI.

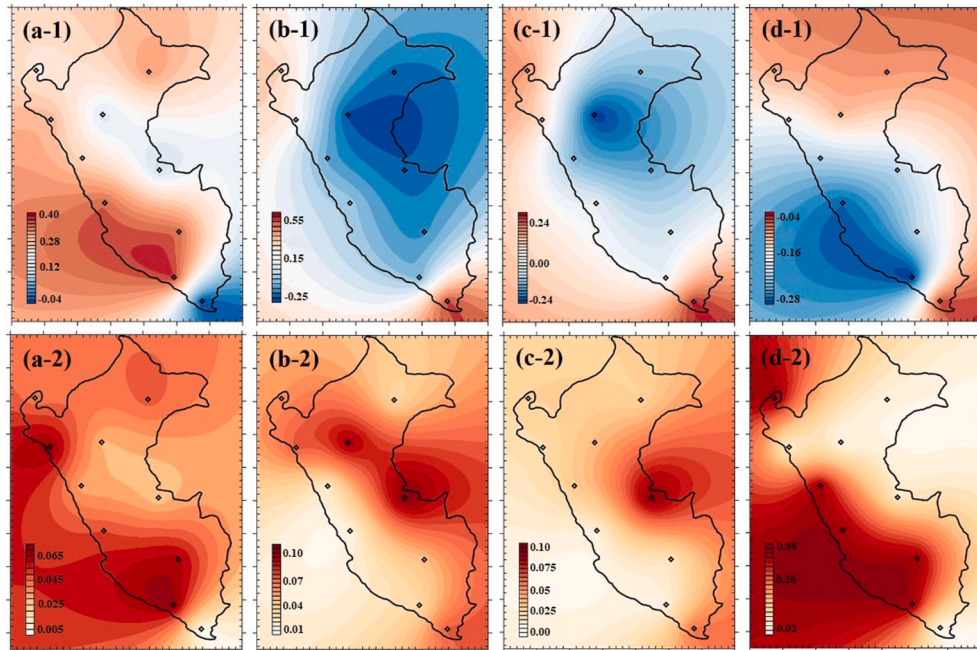


Fig. 9. The relationship between SPI-3 and NAO (a), ENSO (b), PDO (c), and AMO (d) by considering the (1) PCC and (2) MI.

the results obtained by Bendix et al. (2000) for the 1991–1992 El Niño event, Rodríguez-Morata et al. (2019) for El Niño event 1997–1998, and Lagos et al. (2008) for El Niño events between 1950 and 2002. However, there are also several cases in which all the selected oscillations had positive phases, e.g. July 997 in LSR, June 2007 in SAM and UCA, but no extreme event occurred. It is noteworthy that no extreme events took place while all the oscillations were at their negative phases. The figure also shows that the probability of moderately dry conditions between May–August is higher, while extreme droughts are expected to emerge in June and July. In general, February and March were the wettest and the June and July were the driest months within the country. Based on the location and the microclimate of the region, several deviations

occurred. Clearly, the extreme drought conditions are occurring more frequently in 2014 and 2015 and this can be an early warning for future drought events. In this respect, the effect of large-scale oscillations is obvious while the MI shows comparable patterns in a more informative way.

5. Conclusion

The PCC and MI analysis together with the kriging spatial interpolation were used to evaluate the teleconnection between the oceanic oscillations (NAO, ENSO, PDO, and AMO) and the precipitation pattern across Peru during the period of 1990–2015. For this purpose, monthly

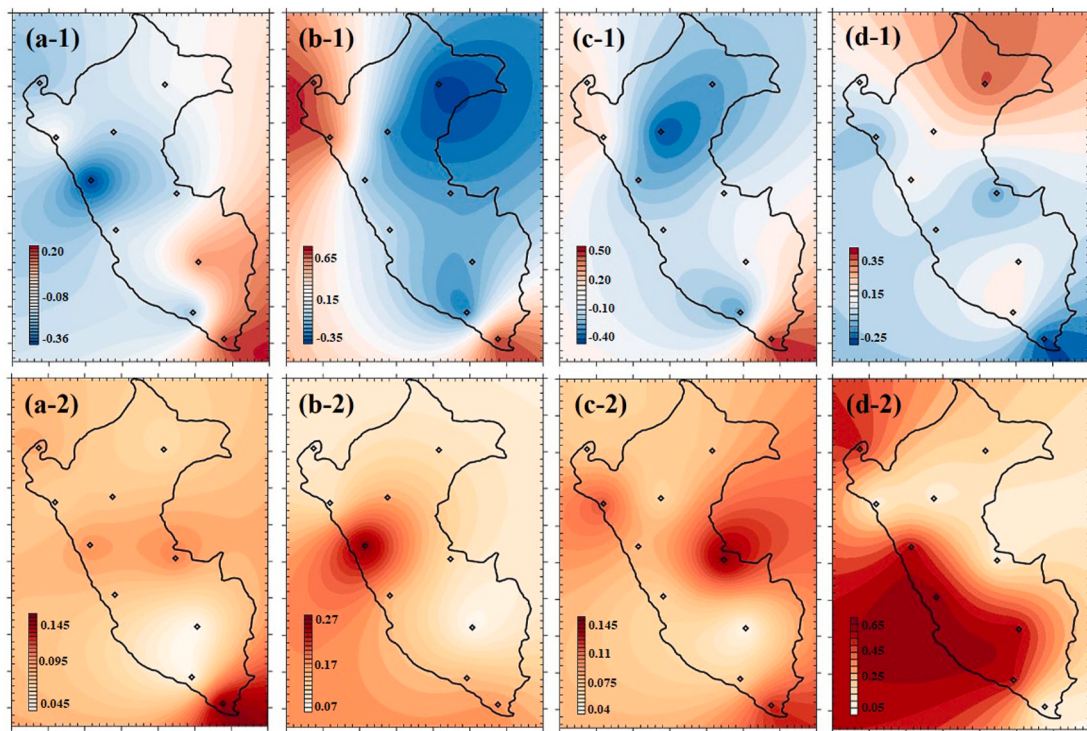


Fig. 10. The relationship between SPI-12 and NAO (a), ENSO (b), PDO (c), and AMO (d) by considering the (1) PCC and (2) MI.

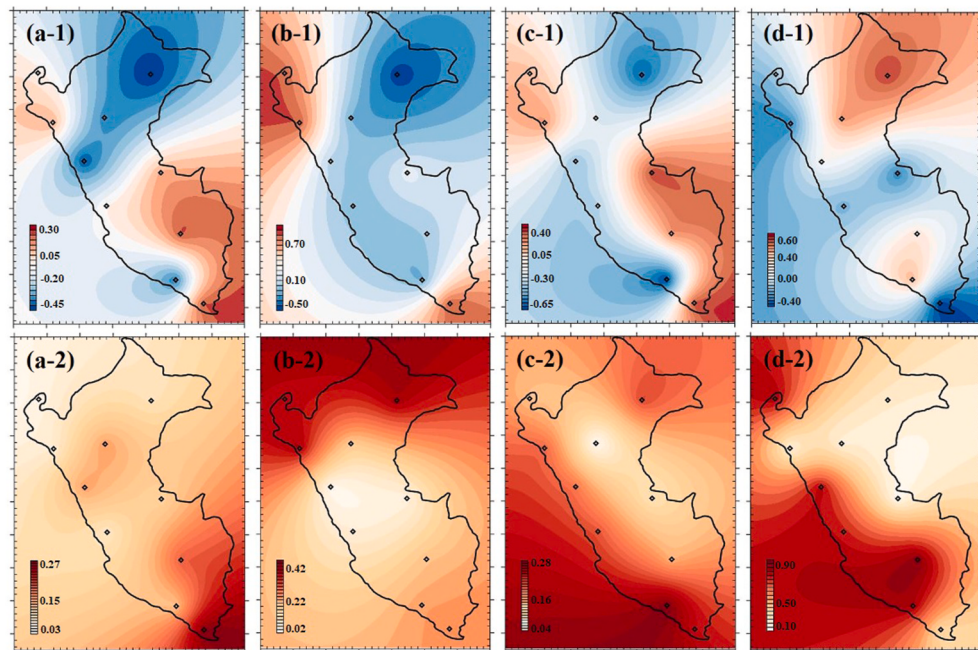


Fig. 11. The relationship between SPI-48 and NAO (a), ENSO (b), PDO (c), and AMO (d) by considering the (1) PCC and (2) MI.

observed precipitation data from 10 meteorology stations and associated SPI indices were used. The concluding remarks are listed as below:

- i. Mount Andes has a great effect on the climate of the region. This result agrees with the results of Condom et al. (2011), Ochoa et al. (2014), Viale and Nunez (2018), and Vaheddoost (2020) who underlined the importance of Mount Andes on Peruvian precipitations.

- ii. The ENSO oscillation has a major effect on the extreme precipitation events in the south, particularly in San Martin. This result is in total agreement with results obtained by Tapley and Waylen (1990), Bendix et al. (2000), Lagos et al. (2008), Perry et al. (2014), Christidis et al. (2019), and Rodríguez-Morata et al. (2019) who investigated the effect of ENSO on the precipitation patterns in the country.

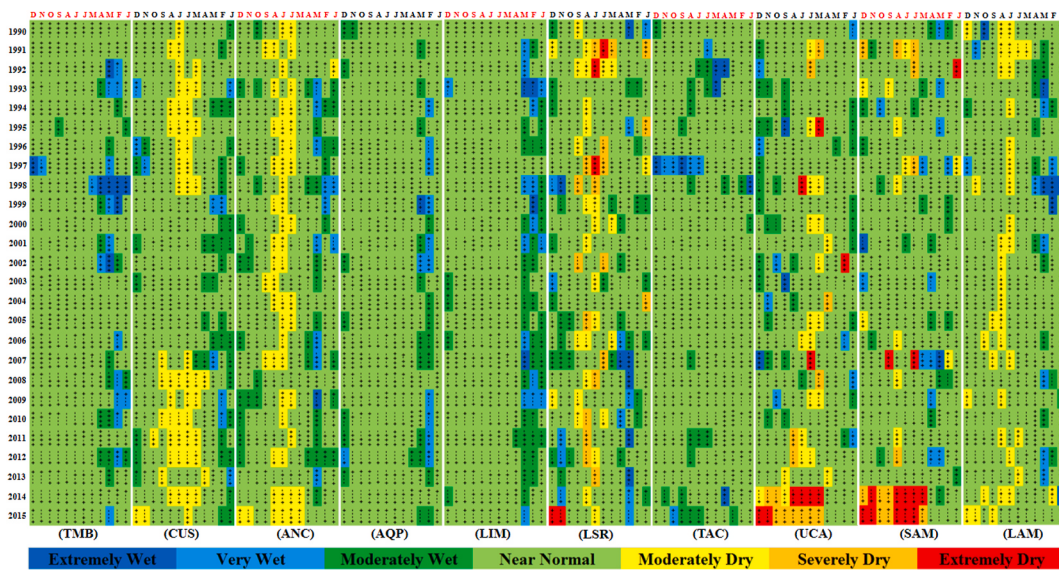


Fig. 12. The temporal relationship between positive (+) and negative (−) phases of the NAO, ENSO, PDO, and AMO respectively (given at the center of each cell) and simultaneously crossed with the SPI-1 events given by.

- iii. The PDO oscillation can also be a trigger for moderate-wet and moderate-dry spells of SPI, however, no significant patterns emerged between AMO and NAO at monthly and annual scales.
- iv. By enlarging the time span from one to 48 months, a significant increase between the SPI and the selected oscillations has been observed. This might be linked to the varying nature of the large-scale oscillations, which slowly but surely alters the drought pattern over the country.
- v. In accordance with the results of [Gonzalez et al. \(2019\)](#), there are signs of accelerating dry spells initiated from late 2014 which can be considered as a signal for climate change, particularly in the Amazon region.

Declaration of competing interest

The authors declare that they have no known competing financial interests or personal relationships that could have appeared to influence the work reported in this paper.

Acknowledgment

The authors appreciate the Republic of Peru's National Service of Meteorology and Hydrology (SENAMHI) for providing the required data for this study.

References

- Baker, P.A., Seltzer, G.O., Fritz, S.C., Dunbar, R.B., Grove, M.J., Tapia, P.M., et al., 2001. The history of South American tropical precipitation for the past 25,000 years. *Science* 291 (5504), 640–643.
- Beck, H.E., Zimmermann, N.E., McVicar, T.R., Vergopolan, N., Berg, A., Wood, E.F., 2018. Present and future Köppen-Geiger climate classification maps at 1-km resolution. *Scientific data* 5, 180214.
- Bendix, J., 2000. Precipitation dynamics in Ecuador and northern Peru during the 1991/92 El Niño: a remote sensing perspective. *Int. J. Rem. Sens.* 21 (3), 533–548.
- Christidis, N., Betts, R.A., Stott, P.A., 2019. The extremely wet March of 2017 in Peru. *Bull. Am. Meteorol. Soc.* 100 (1), S31–S35.
- Condom, T., Rau, P., Espinoza, J.C., 2011. Correction of TRMM 3B43 monthly precipitation data over the mountainous areas of Peru during the period 1998–2007. *Hydrol. Process.* 25 (12), 1924–1933.
- Danandeh Mehr, A., Kahya, E., Özger, M., 2014. A gene-wavelet model for long lead time drought forecasting. *J. Hydrol.* 517, 691–699.
- Danandeh Mehr, A., Nourani, V., Hrnjica, B., Molajou, A., 2017. A binary genetic programming model for teleconnection identification between global sea surface temperature and local maximum monthly rainfall events. *J. Hydrol.* 555, 397–406.
- Danandeh Mehr, A., Vaheddoost, B., 2019. Identification of the trends associated with the SPI and SPEI indices in ankara, Turkey. *Theor. Appl. Climatol.* <https://doi.org/10.1007/s00704-019-03071-9>.
- Danandeh Mehr, A., Jabarnejad, M., Nourani, V., 2019. Pareto-optimal MPSA-MGGP: a new gene-annealing model for monthly rainfall forecasting. *J. Hydrol.* 571, 406–415.
- Derin, Y., Nikolopoulos, E., Anagnostou, E.N., 2019. Estimating Extreme Precipitation Using Multiple Satellite-Based Precipitation Products. *Extreme Hydroclimatic Events and Multivariate Hazards in a Changing Environment. A Remote Sensing Approach*, p. 163.
- Gonzalez, F.R., Raval, S., Taplin, R., Timms, W., Hitch, M., 2019. Evaluation of impact of potential extreme rainfall events on mining in Peru. *Nat. Resour. Res.* 28 (2), 393–408.
- Himayoun, D., Roshni, T., 2019. Spatio-temporal variation of drought characteristics, water resource availability and the relation of drought with large scale climate indices: a case study of Jhelum basin, India. *Quat. Int.* 525, 140–150.
- Huang, S., Huang, Q., Chang, J., Zhua, Y., Leng, G., 2015. Drought structure based on a nonparametric multivariate standardized drought index across the Yellow River basin China. *J. Hydrol.* 530 (4), 235–259.
- Kottek, M., Grieser, J., Beck, C., Rudolf, B., Rubel, F., 2006. World map of the Köppen-Geiger climate classification updated. *Meteorol. Z.* 15 (3), 259–263.
- Lagos, P., Silva, Y., Nickl, E., Mosquera, K., 2008. El Niño – related precipitation variability in Peru. *Adv. Geosci.* 14, 231–237.
- Manzanas, R., Gutiérrez, J.M., 2019. Process-conditioned bias correction for seasonal forecasting: a case-study with ENSO in Peru. *Clim. Dynam.* 52 (3–4), 1673–1683.
- McKee, T.B., Doesken, N.J., Kleist, J., 1993. The relationship of drought frequency and duration to time scales. No. 22. In: *Proceedings of the 8th Conference on Applied Climatology*, vol. 17, pp. 179–183. Boston, MA: American Meteorological Society.
- Ochoa, A., Pineda, L., Crespo, P., Willems, P., 2014. Evaluation of TRMM 3B42 precipitation estimates and WRF retrospective precipitation simulation over the Pacific-Andean region of Ecuador and Peru. *Hydrol. Earth Syst. Sci.* 18 (8), 3179–3193.
- Perry, L.B., Seimon, A., Kelly, G.M., 2014. Precipitation delivery in the tropical high Andes of southern Peru: new findings and paleoclimatic implications. *Int. J. Climatol.* 34 (1), 197–215.
- Rodríguez-Morata, C., Díaz, H.F., Ballesteros-Canovas, J.A., Rohrer, M., Stoffel, M., 2019. The anomalous 2017 coastal El Niño event in Peru. *Clim. Dynam.* 52 (9–10), 5605–5622.
- Shimada, I., Schaaf, C.B., Thompson, L.G., Mosley-Thompson, E., 1991. Cultural impacts of severe droughts in the prehistoric Andes: application of a 1,500-year ice core precipitation record. *World Archaeol.* 22 (3), 247–270.
- Setiawan, A.M., Lee, W.S., Rhee, J., 2017. Investigating the relationship between droughts and the phenomenon of Enso. *Int. J. Climatol.* 4 (3), 47–59.
- Tapley Jr., T.D., Waylen, P.R., 1990. Spatial variability of annual precipitation and ENSO events in western Peru. *Hydrol. Sci. J.* 35 (4), 429–446.
- Thompson, L.G., Mosley-Thompson, E., Bolzan, J.F., Koci, B.R., 1985. A 1500-year record of tropical precipitation in ice cores from the Quelccaya ice cap, Peru. *Science* 229 (4717), 971–973.
- Tong, J., Qiang, Z., Deming, Z., Yijin, W., 2006. Yangtze floods and droughts (China) and teleconnections with ENSO activities (1470–2003). *Quat. Int.* 144 (1), 29–37.
- Vaheddoost, B., 2020. A spatiotemporal classification of the Peruvian precipitations between 1990 and 2015. *Pure Appl. Geophys.* 1–12. <https://doi.org/10.1007/s00024-020-02454-8>.
- Vaheddoost, B., 2017. Spatial analysis of large atmospheric oscillations and annual precipitation in Lake Urmia basin. *European Water* 59, 123–129.

- Vazifehkhan, S., Kahya, E., 2019. Hydrological and agricultural droughts assessment in a semi-arid basin: inspecting the teleconnections of climate indices on a catchment scale. *Agric. Water Manag.* 217, 413–425.
- Viale, M., Núñez, M.N., 2018. Climatology of winter orographic precipitation over the subtropical central Andes and associated synoptic and regional characteristics. *J. Hydrometeorol.* 19 (2).
- World Meteorological Organization (WMO), 2012. Standardized Precipitation Index User Guide, ISBN 978-92-63-11091-6. Geneva, Switzerland.
- Yihdego, Y., Vaheddoost, B., Al-Weshah, R.A., 2019. Drought indices and indicators revisited. *Arab. J. Geosci.* 12 (3), 69.
- Zeleke, T., Giorgi, T., Diro, F., Zaitchik, B., 2017. Trend and periodicity of drought over Ethiopia. *Int. J. Climatol.* 65 (4), 33–48.
- Zubieta, R., Getirana, A., Espinoza, J.C., Lavado, W., 2015. Impacts of satellite-based precipitation datasets on rainfall-runoff modeling of the Western Amazon basin of Peru and Ecuador. *J. Hydrol.* 528, 599–612.
- Zubieta, R., Saavedra, M., Silva, Y., Giráldez, L., 2017. Spatial analysis and temporal trends of daily precipitation concentration in the Mantaro River basin: central Andes of Peru. *Stoch. Environ. Res. Risk Assess.* 31 (6), 1305–1318.
- Zubieta, R., Saavedra, M., Espinoza, J.C., Ronchail, J., Sulca, J., Drapeau, G., Martin-Vide, J., 2019. Assessing precipitation concentration in the Amazon basin from different satellite-based data sets. *Int. J. Climatol.* 39 (7), 3171–3187.